



Antibacterial conductive self-healing hydrogel wound dressing with dual dynamic bonds promotes infected wound healing

Lipeng Qiao^{a,1}, Yongping Liang^{a,1}, Jueying Chen^a, Ying Huang^a, Saeed A. Alsareii^{c,d,**}, Abdulrahman Manaa Alamri^c, Farid A. Harraz^d, Baolin Guo^{a,b,e,*}

^a Key Laboratory of Shaanxi Province for Craniofacial Precision Medicine Research, College of Stomatology, Xi'an Jiaotong University, Xi'an, 710049, China

^b Frontier Institute of Science and Technology, State Key Laboratory for Mechanical Behavior of Materials, Xi'an Jiaotong University, Xi'an, 710049, China

^c Department of Surgery, College of Medicine, Najran University, Najran, 11001, Saudi Arabia

^d Promising Centre for Sensors and Electronic Devices (PCSED), Advanced Materials and Nano-Research Centre, Najran University, Najran, 11001, Saudi Arabia

^e Department of Orthopaedics, The First Affiliated Hospital of Xi'an Jiaotong University, Xi'an, 710061, China

ARTICLE INFO

Keywords:

Dynamic crosslinking
Self-healing
Infected wound
Photothermal antibacterial
Wound healing

ABSTRACT

In clinical applications, there is a lack of wound dressings that combine efficient resistance to drug-resistant bacteria with good self-healing properties. In this study, a series of adhesive self-healing conductive antibacterial hydrogel dressings based on oxidized sodium alginate-grafted dopamine/carboxymethyl chitosan/Fe³⁺ (OSD/CMC/Fe hydrogel)/polydopamine-encapsulated poly(thiophene-3-acetic acid) (OSD/CMC/Fe/PA hydrogel) were prepared for the repair of infected wound. The Schiff base and Fe³⁺ coordination bonds of the hydrogel structure are dynamic bonds that can be repaired automatically after the hydrogel network is disrupted. Macroscopically, the hydrogel exhibits self-healing properties, allowing the hydrogel dressing to adapt to complex wound surfaces. The OSD/CMC/Fe/PA hydrogel showed good conductivity and photothermal antibacterial properties under near-infrared (NIR) light irradiation. In addition, the hydrogels exhibit tunable rheological properties, suitable mechanical properties, antioxidant properties, tissue adhesion properties and hemostatic properties. Furthermore, all hydrogel dressings improved wound healing in the infected full-thickness defect skin wound repair test in mice. The wound size repaired by OSD/CMC/Fe/PA3 hydrogel + NIR was much smaller (12%) than the control group treated with Tegaderm™ film after 14 days. In conclusion, the hydrogels have high antibacterial efficiency, suitable conductivity, great self-healing properties, good biocompatibility, hemostasis and antioxidant properties, making them promising candidates for wound healing dressings for the treatment of infected skin wounds.

1. Introduction

The skin is an essential part of the human body, which is responsible for protecting people from external aggressions, regulating body temperature, sensing external stimuli and so on [1,2]. At the same time, since the skin is exposed to the outside world, it is vulnerable to external aggression. Once the skin is damaged, its healing requires a complex and lengthy process that involves hemostasis, inflammation, hyperplasia and wound remodeling with the formation of scar tissue [3]. In order to

promote wound healing, various biomaterials have been developed, such as electrospun fiber [4], foams and sponges [5,6], films [6], and hydrogels [7]. In particular, hydrogel has a three-dimensional network structure, wound exudate absorption performance, moisturizing ability and oxygen permeability, and has a wide range of promising application in the area of wound dressing. Besides, movement of the wound site can cause tearing or even damage to the dressing, which requires good self-healing properties of the dressing. However, existing hydrogel dressings are difficult to meet the demand, hence, there is a need to

Peer review under responsibility of KeAi Communications Co., Ltd.

* Corresponding author. Key Laboratory of Shaanxi Province for Craniofacial Precision Medicine Research, College of Stomatology, Xi'an Jiaotong University, Xi'an, 710049, China.

** Corresponding author. Department of Surgery, College of Medicine, Najran University, Najran, 11001, Saudi Arabia.

E-mail addresses: alsareii@nu.edu.sa (S.A. Alsareii), baoling@mail.xjtu.edu.cn (B. Guo).

¹ These authors contributed equally to this work.

<https://doi.org/10.1016/j.bioactmat.2023.07.015>

Received 13 February 2023; Received in revised form 2 July 2023; Accepted 18 July 2023

2452-199X/© 2023 The Authors. Publishing services by Elsevier B.V. on behalf of KeAi Communications Co. Ltd. This is an open access article under the CC BY-NC-ND license (<http://creativecommons.org/licenses/by-nc-nd/4.0/>).

design a hydrogel wound dressing with good self-healing properties. Hydrogels with self-healing properties are usually constructed through dynamic chemical bonds. The Schiff base bond is most widely used to build dynamic networks, which are stronger than disulfide bonds and acylhydrazone [8], and it also has the advantages of mild reaction conditions, fast reaction rate, and suitability for biological materials. On the other hand, metal coordination bond is another common used dynamic chemical bond, among which Fe^{3+} and catechol are relatively common metal coordination systems [9]. The metal coordination bond between catechol and Fe^{3+} can effectively dissipate mechanical energy and is considered as a sacrificial bond for load dispersion and impact absorption [10], can endow the material with good self-healing performance. In conclusion, introducing metal ion coordination bond and Schiff base bond into hydrogel network enables the design of hydrogel with good self-healing properties.

Natural biomacromolecule sodium alginate (SA) is often used to construct hydrogel materials, because it has good biocompatibility, abundant carboxyl groups and good solubility [11]. Oxidized sodium alginate (OSA) obtained by oxidizing sodium alginate has an aldehyde group [12], which can greatly improve the ability of SA to cross-link with other molecules. Dopamine (DA) is a substance secreted by mussels that is highly adhesive [13]. Thus, the tissue adhesion of OSA was further improved by grafting DA. In addition, DA can also provide antioxidant, metal coordination and hemostatic properties to dressing [14]. This DA-grafted-OSA (OSD) with multiple functions was chosen to construct the hydrogel network in this study.

Chitosan is the product of partial deacetylation of natural polysaccharide chitin [15]. It has functions such as biodegradability, biocompatibility and antibacterial. Further, it is one of the most widely used biological macromolecules [16]. Yet, its application is limited by the poor water solubility of chitosan [17]. Carboxymethyl chitosan (CMC) enhances chitosan's solubility in water by introducing a certain number of hydrophilic carboxyl groups. In addition, the remaining amino groups in CMC can also react with aldehyde groups of the above OSD. Based on the above discussion, CMC and OSD were selected to construct the first dynamic Schiff base network. In addition, the addition of Fe^{3+} coordinates with the carboxyl groups and catechol in OSD to form the second dynamic bond—metal coordination bond [18]. These dual dynamic bonds crosslinked network will endow the hydrogel with good mechanical and self-healing properties.

Bacterial infection is another problem in wound repair that can lead to the formation of chronic wounds and the effectiveness of commonly used antibiotics is greatly reduced by the presence of drug-resistant bacteria. So, it is vital to design hydrogel dressings with good antibacterial properties. To construct an effective antibacterial hydrogel, a robust antibacterial strategy must be selected. Common non-antibiotic antibacterial agents against bacteria include metal ion antibacterial agents, natural biological macromolecular antibacterial agents and photothermal antibacterial agents [19]. The application of metal ion antibacterial agents has been limited to some extent due to their potential cytotoxicity and relatively high price [20]. Although natural biomacromolecules such as chitosan have certain antibacterial properties, they are difficult to deal with severe infection of biofilms [21]. As a new antibacterial strategy, photothermal antibacterial treatment kills bacteria by using the extremely strong penetrating power of near-infrared light, thereby solving the problem of serious infections [22]. Realization of photothermal antibacterial requires adding photothermal agent to the material. As a photothermal agent with good biocompatibility, chemical stability and photothermal properties [23, 24], the application of poly(thiophene-3-acetic acid) (PTAA) to antibacterial wound dressings is promising. However, its water solubility is insufficient. Fortunately, polymerizing dopamine on the surface of PTAA to form polydopamine-coated PTAA (PA) can improve the hydrophilicity of PTAA, and its photothermal properties was also further improved due to the addition of polydopamine (PDA). On the other hand, PTAA, as a conducting polymer, can also impart conductivity to

hydrogel dressing. Conductive dressings may promote wound healing by enhancing electrical signal exchange between cells [25]. Overall, the introduction of PA into the hydrogel can enable it with both high-efficiency antibacterial properties and conductivity.

Overall, this study developed a multifunctional hydrogel with good antibacterial and self-healing properties based on OSD, CMC, Fe^{3+} and PA, and applied it to the repair of infected full-thickness defect skin wounds. The hydrogel initially forms a cross-linked network by forming Schiff bases between OSD and CMC, and then the hydrogel network was further strengthened by adding FeCl_3 . Meanwhile, the addition of PA to the hydrogel enhances its conductivity, photothermal properties and tissue adhesion. In this study, the hydrogels were systematically tested for their photothermal antimicrobial properties, conductivity, self-healing properties, adhesion and hemostatic properties, and a mouse infected full-thickness defect skin wound model was finally selected to comprehensively evaluate the performance of multifunctional OSD/CMC/ Fe^{3+} /PA (OSD/CMC/Fe/PA) hydrogel as a wound dressing. In this study, these multifunctional hydrogel dressings were shown to have good properties and show good promise in the treatment of bacterially infected skin wounds.

2. Results and Discussion

In this research, a range of self-healing antibacterial conductive hydrogel dressings with dual dynamic bonds and suitable mechanical properties, conductivity, photothermal properties, antioxidant properties, self-healing properties, and biocompatibility were prepared, and the evaluation of their application in the treating of infected wounds were also demonstrated. The general strategy for designing the hydrogel for wound healing is shown in Fig. 1. Sodium alginate (SA) was selected as the main network molecule because it has good biocompatibility and coordination properties with metals. In order to give SA an aldehyde group, sodium periodate was used to oxidize sodium alginate to obtain OSA (Fig. 1a). The appearance of two peaks with $\delta = 4.9$ and 5.0 in the ^1H NMR spectrum proved the successful synthesis of OSA (Fig. S4). In order to impart good adhesion and antioxidant to OSA, dopamine (DA) was linked to OSA by classical 1-(3-dimethylaminopropyl)-3-ethylcarbodiimide hydrochloride (EDC)/N-hydroxysuccinyl Imine (NHS) chemistry to synthesize dopamine-grafted oxidized sodium alginate (OSD) (Fig. 1a). The appearance of the benzene ring peak ($\delta = 6.9$) (Fig. S4) on the ^1H NMR spectrum of OSD proves the successful grafting of dopamine. PTAA, which has conductive properties, was coated with polydopamine (PDA) to improve its water solubility as well as photothermal properties (Fig. 1b), and at the same time, PDA can also increase tissue adhesion. To introduce Schiff base bonds in the hydrogel network, carboxymethyl chitosan was chosen as another main component (Fig. 1c). As a chemically modified molecule of chitosan, carboxymethyl chitosan has good water solubility and biocompatibility, it also contains carboxyl and amino groups, and can form Schiff base bonds with OSD and coordinate with metal ions. Next, in order to further strengthen the network of the hydrogel, Fe^{3+} ions were introduced to coordinate with carboxyl groups in CMC and catechol groups in dopamine (Fig. 1c). In the Fourier Transform Infrared (FTIR) spectra (Fig. S5), the successful preparation of OSD is demonstrated by the aldehyde peak at 1733 cm^{-1} , the benzene ring peak at $950\text{--}650\text{ cm}^{-1}$ and the C–N bond peak at 1400 cm^{-1} . The carboxylic acid peak at 1705 cm^{-1} , the thiophene ring peak at $1200\text{--}1050\text{ cm}^{-1}$ and the benzene ring peak at $950\text{--}650\text{ cm}^{-1}$ of PA also proved the successful preparation of PA. The FTIR spectra of the OSD/CMC/Fe/PA hydrogels showed the superposition of the carboxylate, Schiff base and amide peaks at 1590 cm^{-1} and the hydroxyl peak in the sugar ring at 1050 cm^{-1} . Finally, a series of multifunctional antibacterial OSD/CMC/Fe/PA hydrogel dressings were constructed for the repair of infected full-thickness skin wound models in mice (Fig. 1c). The different hydrogels were named as OSD/CMC, OSD/CMC/Fe, OSD/CMC/Fe/PA1 (1 wt% PA), OSD/CMC/Fe/PA3 (3 wt% PA), and OSD/CMC/Fe/PA5 (5 wt% PA) according to the presence or absence of Fe^{3+}

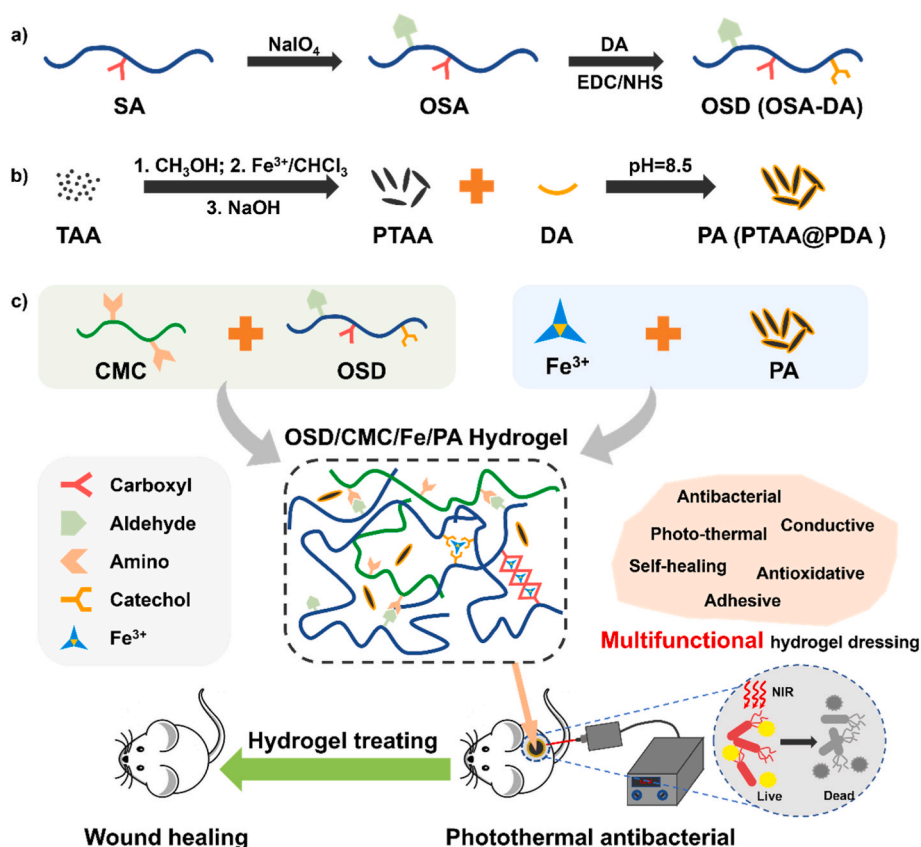


Fig. 1. a) Preparation scheme of oxidized sodium alginate-grafted dopamine (OSD) and b) polydopamine-coating poly(thiophene-3-acetic acid) (PA); c) Preparation and application of OSD/carboxymethyl chitosan/ Fe^{3+} /PA (OSD/CMC/Fe/PA) hydrogels.

and the amount of PA added.

2.1. Rheological properties, morphology, swelling properties, degradation properties and conductivity of hydrogels

Fig. 2a shows a picture of the preparation of the hydrogel. The OSD/CMC/Fe/PA hydrogel can be formed by mixing the CMC solution with the OSD/ Fe^{3+} /PA mixture. The storage modulus (G') and loss modulus (G'') of a series of hydrogels were recorded as a function of time to examine the effect of different PA contents on the modulus of OSD/CMC/Fe/PA hydrogels (Fig. 2b). The G' of the OSD/CMC/Fe/PA5 hydrogel with 5 wt% PA (120.9 Pa) was higher than the values obtained for hydrogel with PA 3 wt% (104.9 Pa), 1 wt% (94.8 Pa) and 0 wt% (77.4 Pa) and OSD/CMC hydrogel (44.2 Pa). This is because the addition of Fe^{3+} and the increase of PA content led to the increase of the cross-linking density of the hydrogel, which in turn led to the gradual increase of the G' of the hydrogel.

The morphology of these OSD/CMC/Fe/PA hydrogels were observed by scanning electron microscopy (SEM) (Fig. 2c). The pore size of the hydrogel is negatively correlated with the amount of PA added, that is, with the increase of the amount of PA, the pore size of the hydrogel gradually decreases. It is introduced that the network of the hydrogel strengthens step by step with PA added, thereby forming a smaller pore size.

The swelling ratio is an important parameter for hydrogels [26]. By absorbing wound exudate, the hydrogel effectively reduces infection, resulting in faster wound healing [27]. Fig. 2d shows the swelling ratio of these hydrogels. Among them, OSD/CMC hydrogel has the highest swelling ratio, reaching 320%. The network of OSD/CMC/Fe hydrogel was further enhanced by the addition of Fe^{3+} to form metal coordination bonds, and the swelling ratio decreased to 288%. Furthermore, the networks of OSD/CMC/Fe/PA1 hydrogel, OSD/CMC/Fe/PA3 hydrogel

and OSD/CMC/Fe/PA5 hydrogel were gradually enhanced with increasing the amount of PA, and the swelling ratio decreased from 266% to 249% and 240%, respectively. The experimental results showed that the swelling ratio of the hydrogel gradually decreased with the addition of Fe^{3+} and PA, which proved the enhancement of the hydrogel network to some extent.

Appropriate degradation rate is important for biomaterials [28]. The results in Fig. 2e show that the OSD/CMC hydrogel was completely degraded in less than 30 h due to the single Schiff base network. But the network of OSD/CMC/Fe hydrogel was strengthened after the addition of Fe^{3+} , which lead to itself completely degraded within 35 h. Furthermore, with the addition of PA, the degradation time of OSD/CMC/Fe/PA1 hydrogel, OSD/CMC/Fe/PA3 hydrogel and OSD/CMC/Fe/PA5 hydrogel increased from 41 h to 59 h and 63 h, respectively. It was shown that the amount of Fe^{3+} and PA nanoparticles increased the strength of the cross-linked network of the hydrogel.

PTAA has good conductivity, biocompatibility and chemical stability, so it was selected as the conductive component to endow these OSD/CMC/Fe/PA hydrogels with conductive properties. Conductive biomaterials have potential to accelerate wound healing [25]. The conductivity of these hydrogels is shown in Fig. 2f. OSD/CMC hydrogel has the lowest conductivity ($3.0 \times 10^{-4} \text{ S m}^{-1}$), however OSD/CMC/Fe hydrogel has an increased conductivity ($3.43 \times 10^{-4} \text{ S m}^{-1}$) due to the addition of Fe^{3+} . Benefit from the addition of conductive nanoparticles PA, the conductivity of OSD/CMC/Fe/PA1 hydrogel, OSD/CMC/Fe/PA3 hydrogel and OSD/CMC/Fe/PA5 hydrogel increased from $5.0 \times 10^{-4} \text{ S m}^{-1}$ to $5.7 \times 10^{-4} \text{ S m}^{-1}$ and $7.2 \times 10^{-4} \text{ S m}^{-1}$, respectively. Dressings with conductive properties will enhance endogenous electrical currents in the skin, thereby causing neutrophils, macrophages, and keratinocytes to migrate to the wound site, which in turn accelerates wound healing [25], therefore, these conductive wound dressings show similar conductivity to skin will be favorable for wound healing.

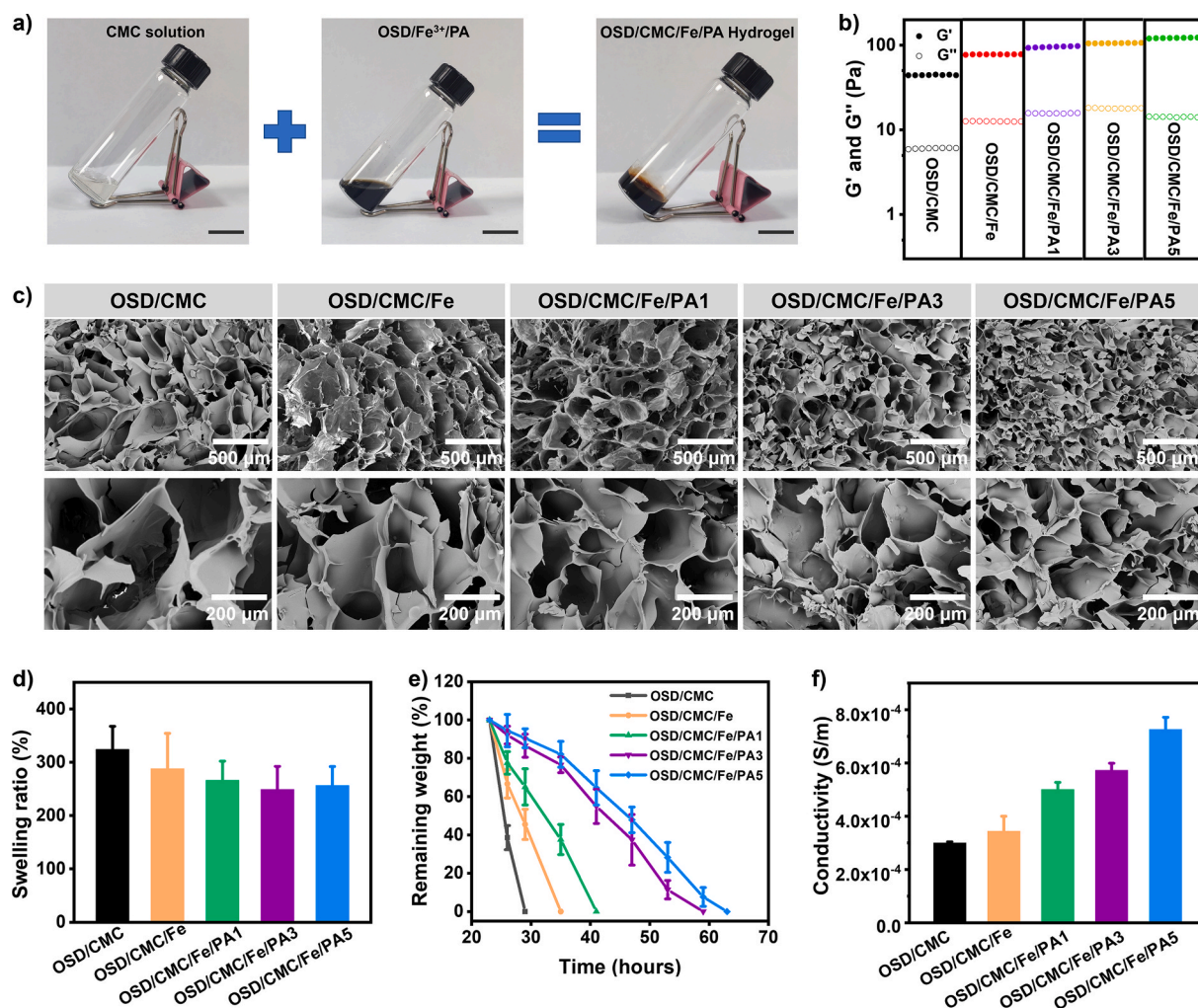


Fig. 2. a) Photographs pictures of hydrogel formation. Scale bar: 2 cm; b) Modulus of hydrogels, the scanning time for each group is 300 s; c) SEM images of hydrogels; d) Swelling ratio and e) degradation of hydrogels in PBS with at 37 °C, pH = 7.4; f) Conductivity of hydrogels.

2.2. Self-healing properties of the hydrogel

Dressings covering wounds surface can easily be damaged by skin movement, thus failing to heal the wound or even causing wound infection. The self-healing hydrogel wound dressing repairs the broken part of the dressing by self-healing behavior, so that the dressing can treat and protect the wound for an extended period of time [29]. OSD/CMC/Fe/PA3 hydrogel was chosen as a representation to test the self-healing properties of the hydrogel. Fig. 3a shows macro-level self-healing performance of the OSD/CMC/Fe/PA3 hydrogel. The OSD/CMC/Fe/PA3 hydrogel was sliced in half, and then these hydrogels were carried out in close contact. After 10 min at 25 °C, the two hydrogels healed into a complete hydrogel. The dual dynamic network hydrogels with ligand and Schiff base bonds of the hydrogel are the source of good automatic repair ability [30,31].

OSD/CMC/Fe/PA3 hydrogels were tested at the rheological level to further examine their self-healing properties [32]. The results in Fig. 3b show that G' of the hydrogel is equal to G'' when the strain reaches 273.2%, indicating that at this strain, the hydrogel is in between solid and liquid state. After the critical strain (strain >273.2%), the hydrogel is completely destroyed. The self-recovery ability of the hydrogel was subsequently performed with the use of successive step-strain tests (Fig. 3c). At the first 300% strain, G' was markedly reduced from 108 Pa to 21 Pa and the hydrogel network was proven to collapse. At the first small strain of 1%, G' recovered to 101 Pa, suggesting most of the cross-linked network of the hydrogel had been recovered. After six high

and low strain cycles tested, the healed hydrogels showed similar G' and G'' values as the first cycle, confirming the great self-healing properties of the OSD/CMC/Fe/PA3 hydrogels.

2.3. Antioxidant, adhesion, hemostatic and coagulation properties of hydrogels

Because of wound infection, a sustained inflammatory response occurs at the wound site, generating a large number of free radicals [33]. This leads to oxidative stress, which further allows for cellular enzyme inactivation, lipid peroxidation, and DNA damage at the wound site [34]. It has been shown that the addition of antioxidant ingredients to wound dressings can significantly reduce the production of free radicals at the wound site to accelerate wound closure [33]. 1, 1-diphenyl-2-trinitrophenylhydrazine (DPPH) is a stable free radical. In this study, the ability of a series of hydrogels to eliminate DPPH was tested, and vitamin C (VC), which has excellent antioxidant properties, was used as a positive control to evaluate its antioxidant properties [35]. The results in Fig. 4a show that these hydrogels have nice antioxidant properties because of the presence of dopamine, while in OSD/CMC/Fe hydrogels the antioxidant properties are weakened to some extent due to the addition of Fe³⁺. Meanwhile, with the addition of PA nanoparticles, the antioxidant capacity of the hydrogels was further enhanced by the polydopamine contained in the nanoparticles [36]. The DPPH clearance ratio was above 90% for all three hydrogel groups, and the clearance increased with the increase of PA addition. Overall, the excellent

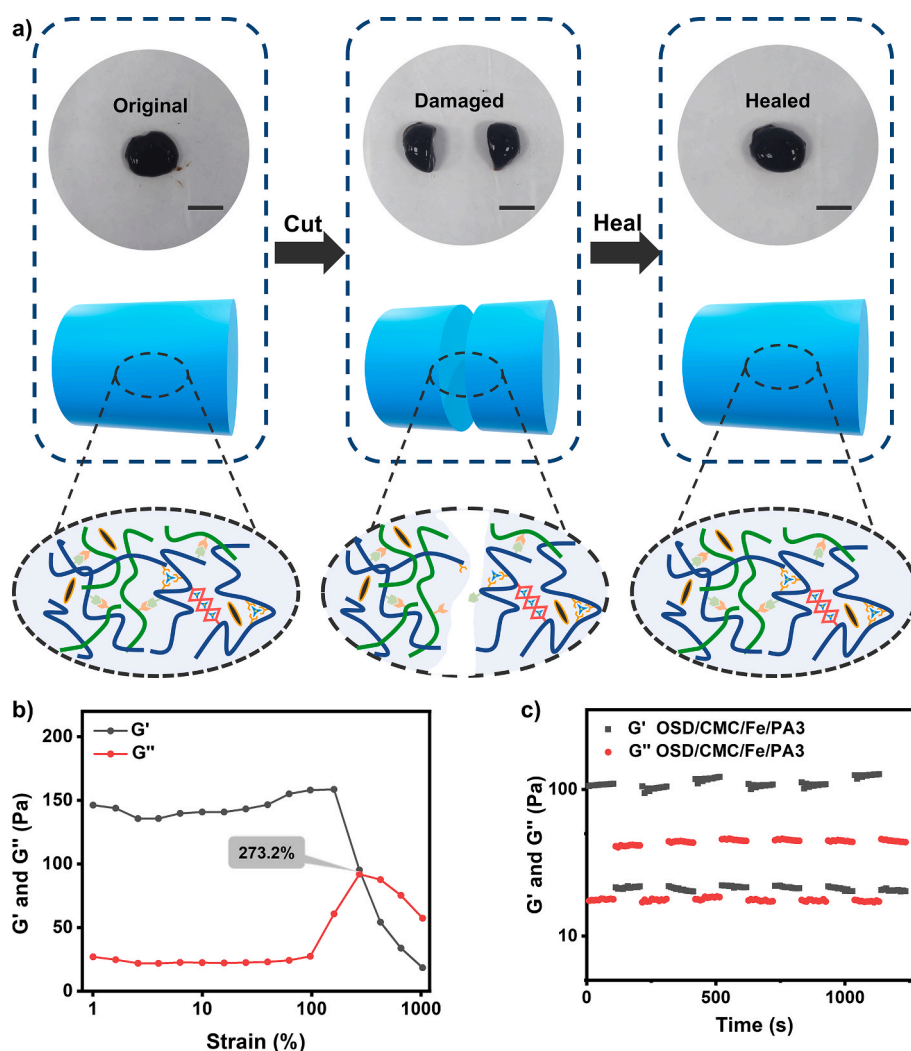


Fig. 3. Self-healing properties of OSD/CMC/Fe/PA3 hydrogel. a) Self-healing demonstration and possible mechanisms of microscopic healing in hydrogels. Scale bar: 1 cm; b) Fracture point testing of the hydrogel; c) Self-healing test of the hydrogel.

antioxidant capacity of OSD/CMC/Fe/PA hydrogels further highlights its advantages as wound dressings.

The activity of these hydrogels to eliminate $\cdot\text{O}_2^-$ was further explored by nitroblue tetrazolium (NBT). As shown in Fig. S8, the hydrogel group with PA had the highest activity of eliminating $\cdot\text{O}_2^-$. Specifically, the $\cdot\text{O}_2^-$ scavenging ratio of OSD/CMC/Fe/PA1, OSD/CMC/Fe/PA3 and OSD/CMC/Fe/PA5 groups was 86.7%, 88.3% and 90.7%, respectively, while the $\cdot\text{O}_2^-$ clearance ratio of OSD/CMC group was 75.9%, and the $\cdot\text{O}_2^-$ scavenging ratio of OSD/CMC/Fe group was the lowest, 63.2%. This showed the same trend as DPPH scavenging test.

A good wound dressing also needs good adhesion in order to adhere tightly to the wound [37]. Since the hydrogel contains a large amount of dopamine, and dopamine is an effective component that provides adhesion properties in the mussel adhesion protein, and the abundant hydrogen bonding in the hydrogel, the hydrogel theoretically has good adhesion ability. In this study, pigskin lap shear tests were carried out to test the adhesive properties of the materials (Fig. 4b&c). All hydrogels have high adhesive strength and their adhesion properties are positively correlated with the amount of PA. Among them, OSD/CMC/Fe/PA3 hydrogels and OSD/CMC/Fe/PA5 hydrogels exhibited better adhesion strength than commercial dressings (~5 kPa), indicating good adhesion properties of the hydrogels. Possible sources of hydrogel adhesion are the Michael reaction of the aldehyde and quinone groups on the OSD and PA with groups such as amino groups of the skin [38], as well as

electrostatic interactions [39], π - π interactions [40] and hydrogen bonding [41] of hydrogels to the skin.

Bleeding is inevitable after a skin injury, especially with a full-thickness defect. Hemostasis is the primary operation in the management of wounds, and rapid hemostasis plays an important role in avoiding massive blood loss [42]. OSD/CMC/Fe/PA hydrogel has several pro-coagulant components, OSD with PA's catechol, CMC's amino and iron ions can promote blood coagulation. In order to explore the hemostasis of hydrogels, the coagulation properties of OSD/CMC/Fe/PA hydrogels was evaluated by dynamic whole blood coagulation assay [32]. Calcified whole blood of rats was used as a control group, and gelatin sponge, a commercially available hemostatic agent, was used as a positive control. Fig. 4d illustrates that a series of hydrogels have a better procoagulant capacity than gelatin sponges. The catechol structure in OSD/CMC/Fe/PA1 and OSD/CMC/Fe/PA3 hydrogels further promotes blood coagulation with a minimum BCI of about 40% due to the introduction of PA. Compared with OSD/CMC/Fe/PA3 hydrogel, the BCI value of OSD/CMC/Fe/PA5 did not change much because the blood absorption capacity was reduced. The above results demonstrate that the newly developed OSD/CMC/Fe/PA3 hydrogel has good coagulation properties.

Based on the procoagulant properties provided by polydopamine and the good tissue adhesion of OSD/CMC/Fe/PA hydrogels, it can be used as a hemostatic agent. To further test the in vivo hemostatic properties of

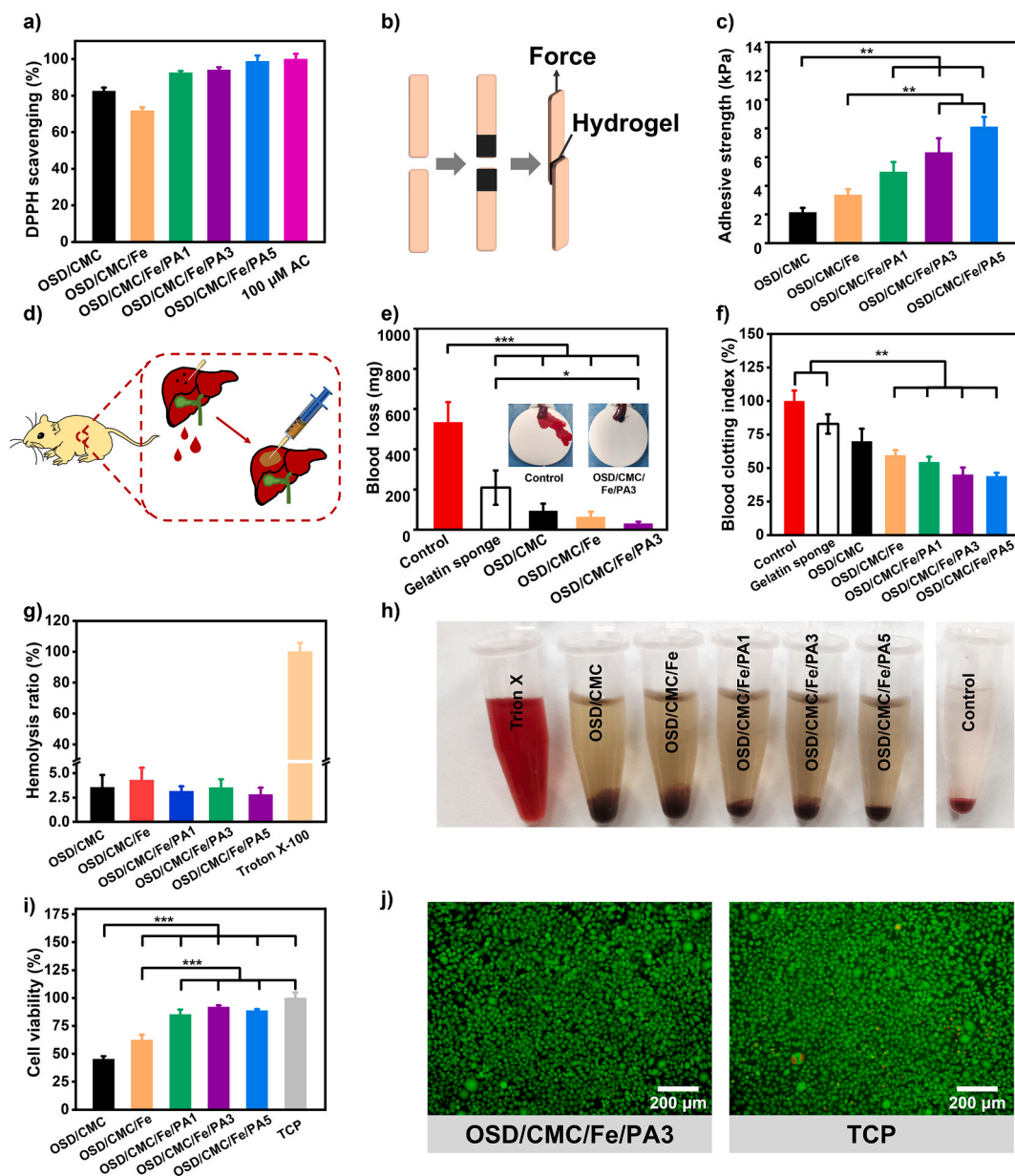


Fig. 4. a) DPPH clearance ratios of different hydrogels; b) Schematic diagram of pigskin adhesion experiment of hydrogels; c) Adhesion strength of pigskin with hydrogel; d) Hemostatic properties of gelatin sponge, OSD/CMC, OSD/CMC/Fe and OSD/CMC/Fe/PA3; e) Schematic diagram of rat liver hemorrhage model; f) Coagulation properties of gauze and hydrogels; g) Hemolytic activity test results of hydrogels; h) Hydrogel hemolytic activity test graphs; i) The cytocompatibility of these hydrogels was assessed by the viability of L929 cells in the hydrogel leachate; j) LIVE/DEAD staining of L929 cells after 24 h of leachate incubation. * $P < 0.05$, ** $P < 0.01$, *** $P < 0.001$.

these dressings, a mouse liver puncture model (Fig. 4e) was constructed to test the hemostatic properties of OSD/CMC/Fe/PA hydrogels [43]. Regardless of the OSD/CMC hydrogel (Fig. 4f), OSD/CMC/Fe hydrogel and OSD/CMC/Fe/PA3 hydrogel, they all had good hemostatic effects, and their blood loss was 90.98 mg, 62.6 mg, and 30.05 mg, respectively, all lower than the commercial gelatin sponge group (209.33 mg) and the control group (532.43 mg). In conclusion, the OSD/CMC/Fe/PA3 hydrogel possessing a good hemostatic ability was chosen as a representative of multifunctional dressing.

2.4. Hemocompatibility and cytocompatibility of hydrogels

The dressing adheres to the wound surface during wound treatment and must have a high level of hemocompatibility from the point of view of biocompatibility [44]. A hemolysis test was chosen to evaluate the

hemocompatibility of the hydrogel. The data in Fig. 4g exhibit a hemolysis ratio of less than 5% (<5% for good hemocompatibility) for the whole hydrogel groups, indicating that the hydrogels have good hemocompatibility.

Cytocompatibility is another important aspect of biocompatibility. Leachate method of L929 cells was selected for testing the cytocompatibility of hydrogels [45]. As shown in Fig. 4i, the OSD/CMC/Fe/PA1 hydrogel and OSD/CMC/Fe/PA3 hydrogel groups have good biocompatibility (cell viability $\geq 80\%$), and the LIVE/DEAD staining diagram in Fig. 4j also confirms the same result.

2.5. Photothermal and photothermal antibacterial properties

Dopamine-encapsulated PA has dual photothermal components, which would have excellent photothermal properties. The change of

hydrogel temperature with irradiation time was tested under 808 nm NIR light irradiation to evaluate its photothermal properties [46]. Fig. 5a represents the pictures of the photothermal performance test. As illustrated in Fig. 5b, the ΔT of OSD/CMC hydrogel is only 3.3 °C after 10 min illumination because there is no photothermal agent added. However, the photothermal performance of OSD/CMC/Fe hydrogel was improved due to the oxidation of dopamine by Fe^{3+} , and its ΔT was found to increase to 17.3 °C. Finally, the OSD/CMC/Fe/PA1, OSD/CMC/Fe/PA3, and OSD/CMC/Fe/PA5 hydrogels with the addition of PA have the best photothermal performance. And with the addition of PA, the ΔT gradually increased, and the ΔT of OSD/CMC/Fe/PA1, OSD/CMC/Fe/PA3, and OSD/CMC/Fe/PA5 hydrogels was 22.5 °C, 23.9 °C, and 25.0 °C, respectively. The photothermal test proved that the OSD/CMC/Fe/PA hydrogels had good photothermal properties.

Stable photothermal properties have important implications for wound dressings. The OSD/CMC/Fe/PA3 hydrogel was selected as a representative hydrogel and the stability of the photothermal properties of the hydrogel was examined by three cycles of photothermal tests at 808 nm at 1.4 W cm^{-2} [14]. The results show that (Fig. 5c) OSD/CMC/Fe/PA3 hydrogel has stable cyclic photothermal performance with the ΔT stable above 23 °C under three cycles. This lays a solid foundation for hydrogels to repair the infected wounds.

Based on the above test results, the photothermal antibacterial ability of these hydrogels were further evaluated by selecting *Escherichia coli* (*E. coli*) and Methicillin-Resistant *Staphylococcus aureus* (MRSA) as

representative bacteria [47]. Fig. 5d is an *in vitro* photothermal antibacterial display photo of OSD/CMC and OSD/CMC/Fe/PA3 hydrogels. Compared with OSD/CMC hydrogel + NIR, OSD/CMC/Fe/PA3 hydrogel + NIR can kill more than 99% of MRSA in about 5 min of light irradiation (Fig. 5e), and can kill all *E. coli* within 10 min (Fig. 5f). Glutaraldehyde fixation of bacteria was performed after photothermal treatment of different hydrogels and SEM images of them were taken. As shown in Fig. S10, the OSD/CMC + NIR treated bacteria exhibited an intact bacterial structure with a smooth bacterial surface, indicating that the bacteria were not significantly damaged. In contrast, after OSD/CMC/Fe/PA3+NIR treatment, both bacteria exhibited irregular morphological shrinkage and increased surface roughness, indicating that the integrity of the bacteria was severely damaged, leading to leakage of contents and protein denaturation. The strong antibacterial performance of OSD/CMC/Fe/PA3 is the result of its excellent photothermal properties and the synergistic effect of antibacterial substances such as carboxymethyl chitosan [48] and Fe^{3+} [49].

An *in vivo* antibacterial test was carried out in a mouse skin wound model infected with MRSA to study the *in vivo* photothermal antibacterial properties of the hydrogel in depth [14]. As shown in Fig. 5g, after different treatments and bacterial cultures of infected tissues, the test results showed high bacterial survival in the control (treated with PBS) and in the wounds treated with OSD/CMC hydrogel, while in the wounds treated with OSD/CMC/Fe/PA3 hydrogel and applying 10 min of NIR irradiation, bacterial survival was extremely low (6.9%). The

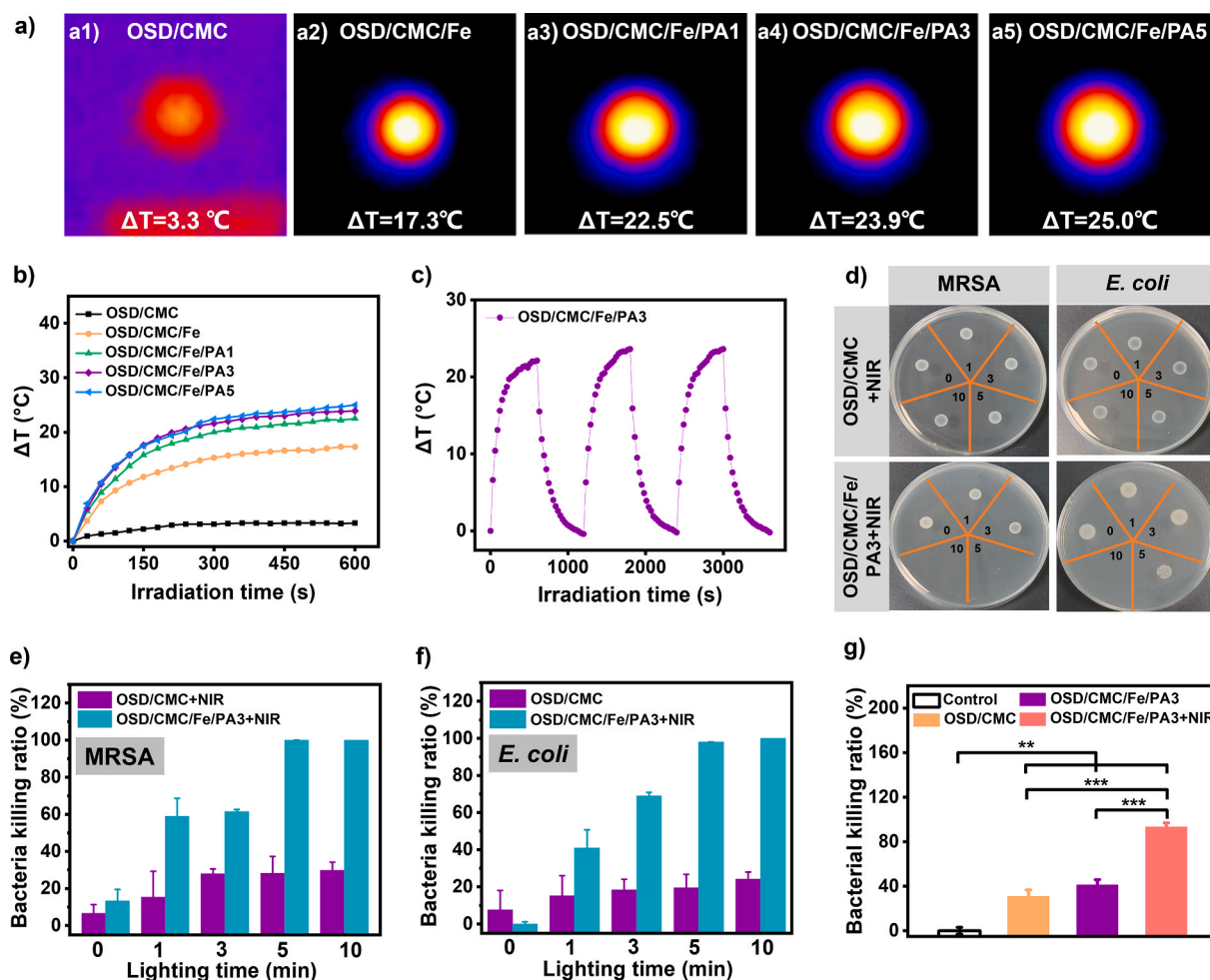


Fig. 5. Heat maps of a1) OSD/CMC, a2) OSD/CMC/Fe, a3) OSD/CMC/Fe/PA1, a4) OSD/CMC/Fe/PA3 and a5) OSD/CMC/Fe/PA5 hydrogels after 10 min of 808 nm NIR radiation; b) ΔT -NIR radiation time curve of the hydrogel under 1.4 W cm^{-2} 808 nm NIR light irradiation; c) Temperature change (ΔT)-irradiation cycle curves of OSD/CMC/Fe/PA3 hydrogels at 1.4 W cm^{-2} light intensity of 808 nm NIR light; d) *In vitro* antibacterial photographs of hydrogels irradiated with NIR light for 0, 1, 3, 5 and 10 min; e) Killing ratio of MRSA and f) *E. coli* for different irradiation time; g) *In vivo* antibacterial results of hydrogels. * $P < 0.05$, ** $P < 0.01$, *** $P < 0.001$.

OSD/CMC/Fe/PA3 hydrogel + NIR group was also significantly different from the other three groups ($P < 0.01$). Furthermore, there was no significant difference in bacterial survival between OSD/CMC and OSD/CMC/Fe/PA3 hydrogel groups, suggesting that the photothermal effect provided by PA and complexes of Fe^{3+} with catechol is the source of the antibacterial properties of OSD/CMC/Fe/PA3.

2.6. In vivo wound healing of MRSA-infected skin full-thickness defect

A mouse full-thickness defect infection model was established to comprehensively evaluate the healing-promoting properties of OSD/CMC/Fe/PA hydrogels as wound dressings [14]. OSD/CMC/Fe/PA3 with good biocompatibility, good conductivity and NIR light-assisted antibacterial properties were selected as experimental group, and Tegaderm™ film commercial product was selected as the control group. As illustrated in Fig. 6, the wound size of the entire group gradually decreased over time. Wounds treated with OSD/CMC hydrogel, OSD/CMC/Fe/PA3 hydrogel and OSD/CMC/Fe/PA3 hydrogel + NIR were all smaller than the control group after 3 days of wound healing. In addition, the wounds treated in the OSD/CMC/Fe/PA3 hydrogel + NIR and OSD/CMC/Fe/PA3 hydrogel groups were significantly different from the OSD/CMC hydrogel and control groups ($P < 0.001$), indicating that the hydrogels with the addition of conductive PTAA had better promotion of repair. After 7 days of wound treatment, all three hydrogel groups had higher wound repair ratio than the control group. After 14 days, the wounds of all groups were largely healed, and the wounds of the hydrogel treatment group were completely closed and even covered by hair. Statistical analysis of the wound area throughout the healing

procedure showed that the wound closure ratio of the OSD/CMC/Fe/PA3 hydrogel and OSD/CMC/Fe/PA3 hydrogel + NIR treatments groups were 95.5% and 97.02%, and 85.01% for the Tegaderm™ film dressing (Fig. 6c). The repair effect of the OSD/CMC/Fe/PA3 hydrogel + NIR group was the best, demonstrating that conductivity and photothermal antibacterial properties can speed up the repair of infected wounds. Overall, the results of these in vivo experiments show that hydrogels with hemostatic, conductive and adhesive properties show great potential for wound healing compared to control.

In the wound repair procedure of inflammation, parenchymal cells have difficulty completing in the repair work. Granulation tissue is very important in the repair process [14]. It completes wound repair by proliferating to dissolve and absorb necrotic tissue and foreign bodies, filling the gaps, and finally transforming into scar tissue. Therefore, the thickness of granulation tissue during wound healing is an important index to assess the effectiveness of wound healing. The results in Fig. 6d show that the granulation tissue thickness in the control group was thinner than all hydrogel groups after 14 days of treatment. In the hydrogel group, the granulation tissue under OSD/CMC/Fe/PA3 hydrogel + NIR treatment was thicker than the OSD/CMC/Fe/PA3 hydrogel group and OSD/CMC hydrogel, while for the OSD/CMC/Fe/PA3 group the thickness of the granulation tissue was thicker than the OSD/CMC hydrogel group. The wound healing effect of all three hydrogel treatment groups was better than that of the control group, with the OSD/CMC/Fe/PA3 hydrogel + NIR group showing the best healing effect.

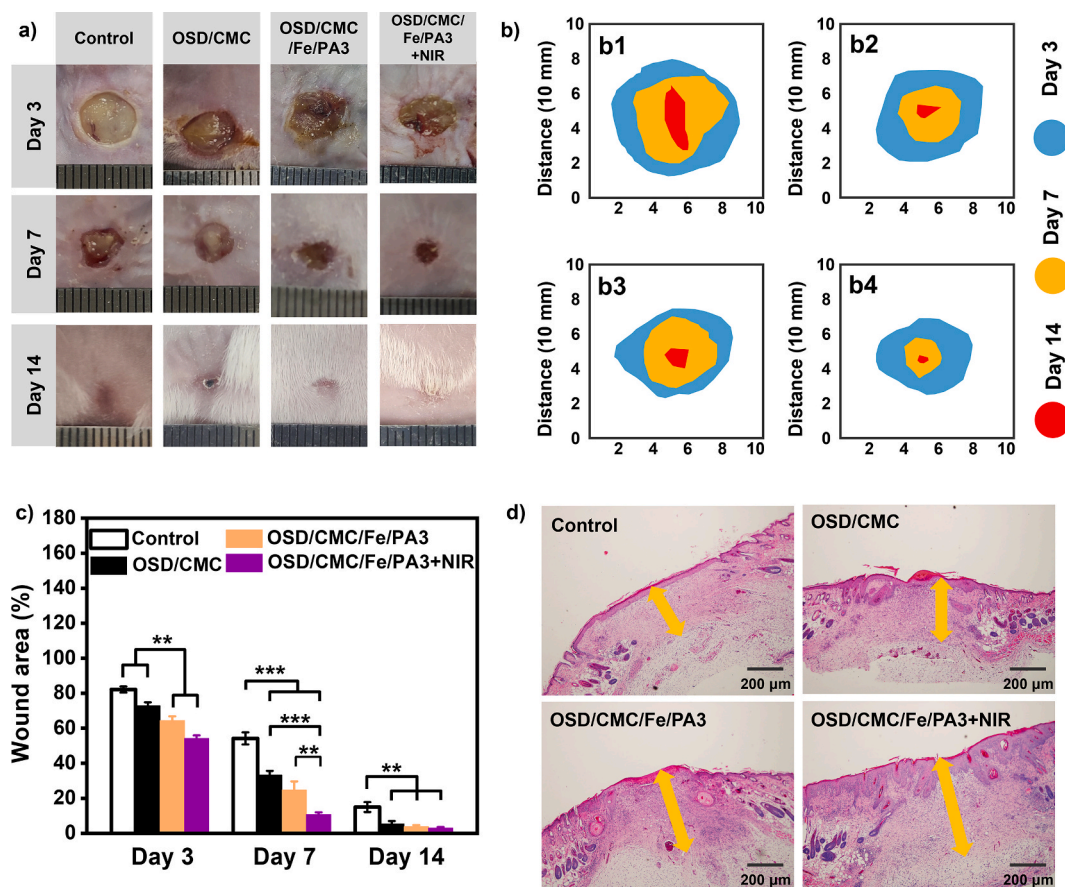


Fig. 6. a) Wound pictures of control group (Tegaderm™ film dressing), OSD/CMC hydrogel, OSD/CMC/Fe/PA3 hydrogel and OSD/CMC/Fe/PA3 hydrogel + NIR on day 3, 7 and 14; b) Schematic diagram of the wound area of b1) control, b2) OSD/CMC hydrogel, b3) OSD/CMC/Fe/PA3 hydrogel, and b4) OSD/CMC/Fe/PA3 hydrogel + NIR for 14 days; c) Wound area of each group; d) Thickness of granulation tissue (orange arrow) in different groups on day 14. * $P < 0.05$, ** $P < 0.01$, *** $P < 0.001$.

2.7. Histomorphological evaluation

Histological analysis was performed on the four experimental groups to assess the repair effect of the regenerated skin at a deeper level (Fig. 7a). Skin of four groups wounds were tested using hematoxylin and eosin (H&E) staining. By comparing the inflammation in the control and hydrogel groups in the initial phase of healing, it was found that the OSD/CMC/Fe/PA3 hydrogel group and the OSD/CMC/Fe/PA3 hydrogel + NIR group had lower levels of inflammation, while the wound site of the control group had a high level of inflammation, and there were more inflammatory cells than in the hydrogel group. The lower inflammation level in the OSD/CMC/Fe/PA3 hydrogel group and the OSD/CMC/Fe/PA3 hydrogel + NIR group may be due to its better antibacterial properties. At day 7, the number of inflammatory cells decreased in all groups. For wound repair, new blood vessels are very important for the function of transporting nutrients, oxygen, enzymes and bioactive factors to the wound tissue site. Fig. 7b shows the statistical results of the number of vessels in each group derived from H&E staining on day 7. The results show that the OSD/CMC/Fe/PA3 group and the OSD/CMC/Fe/PA3 hydrogel + NIR group have more blood vessels than the control group, and the OSD/CMC/Fe/PA3 hydrogel +

NIR group had the most hair follicles. For the day 14 repair results, there were almost no skin appendages although there was intact epithelial cell regeneration in the control group. While the hydrogel-treated wounds, especially the OSD/CMC/Fe/PA3 group and OSD/CMC/Fe/PA3 hydrogel + NIR group hydrogels, had epithelial tissue close to normal skin, and more skin appendages were observed in the whole groups, and have significantly different ($P < 0.01$) compared with the control group. These results suggest that hydrogels, especially those with PA, are beneficial for promoting extracellular matrix (ECM) remodeling and tissue regeneration, and photothermal enhanced antibacterial can effectively eliminate bacteria and accelerate wound healing process. PA imparts conductivity to the hydrogel, which enhances the endogenous current at the wound site, thereby allowing neutrophils, macrophages and keratinocytes to migrate to the wound site, which in turn promotes the regeneration of damaged skin tissue.

2.8. Expression of TNF- α and VEGF during wound healing

Studies have shown that cytokines are involved in the activation and termination of many cellular activities related to repair during wound healing [28]. The level of tumor necrosis factor- α (TNF- α) at the wound

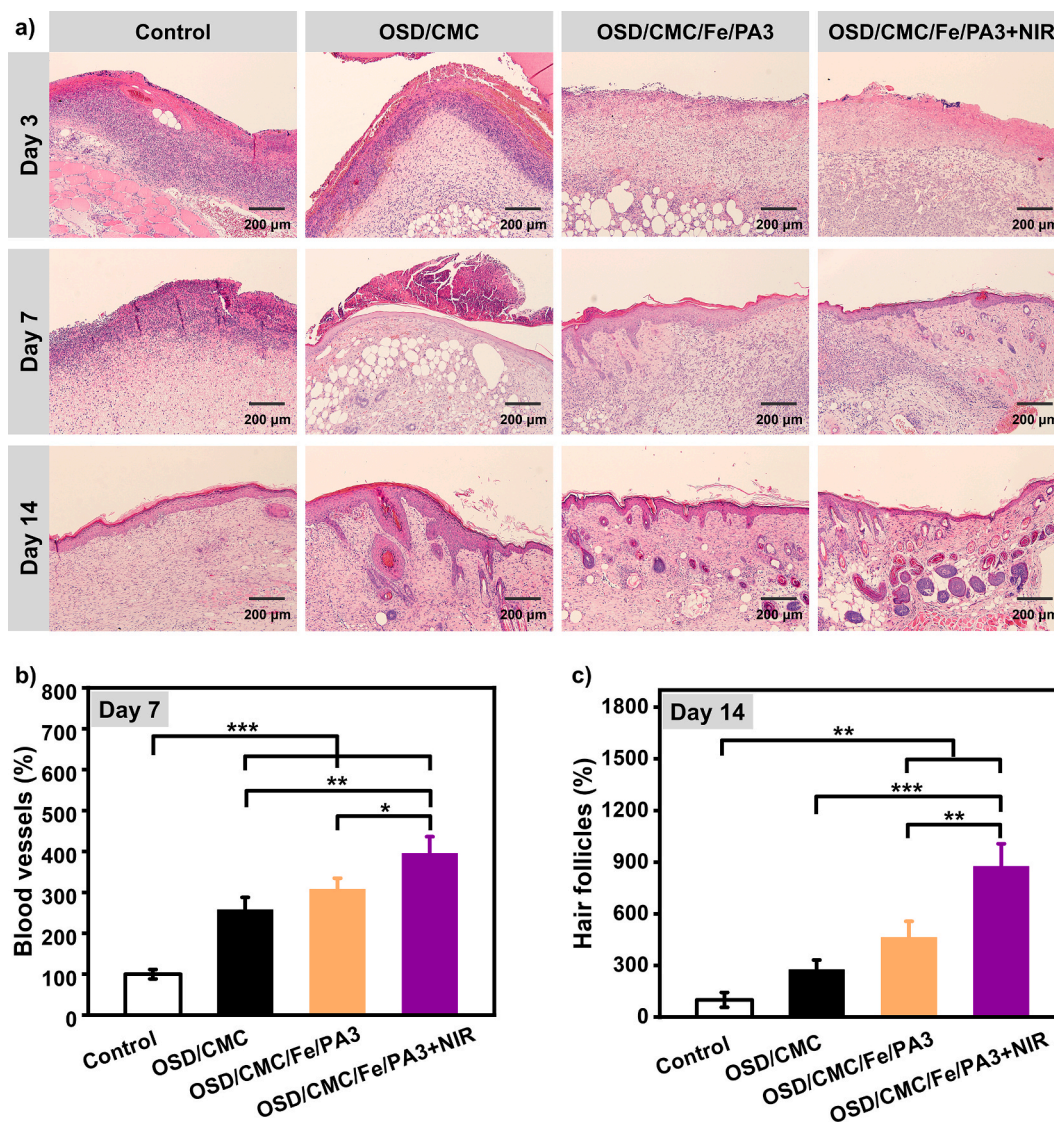


Fig. 7. a) Pictures of histological analysis of wound regeneration on day 3, 7 and 14 of control group (Tegaderm™ film dressing), OSD/CMC hydrogel group, OSD/CMC/Fe/PA3 hydrogel group and OSD/CMC/Fe/PA3 hydrogel + NIR group; b) Statistical graph of angiogenesis on day 7; c) Statistical graph of hair follicles in different groups on 14th day, * $P < 0.05$, ** $P < 0.01$, *** $P < 0.001$.

site can reflect the level of tissue inflammation to some extent [50], so TNF- α was chosen to assess the inflammation of wounds with different groups. In Fig. 8a and c, the OSD/CMC/Fe/PA3 hydrogel + NIR group had the least amount of TNF- α compared with all other groups, proving the good antibacterial properties of OSD/CMC/Fe/PA3 hydrogel + NIR can effectively reduce the inflammation caused by infection. The OSD/CMC hydrogel group and the OSD/CMC/Fe/PA3 hydrogel group were also significantly different from the control group ($p < 0.001$), confirming that these hydrogels outperformed the control group. In this research, the amount of angiogenesis at the wound site was assessed by immunohistochemical staining of the wound for vascular endothelial growth factor (VEGF) at day 7 of wound healing [51]. Fig. 8b&d shows that the wounds treated with OSD/CMC/Fe/PA3 hydrogel + NIR and OSD/CMC/Fe/PA3 hydrogel had significantly higher level of VEGF at day 7 than the control group ($p < 0.001$), indicating that the addition of conductive antibacterial component PA has advantages in promoting angiogenesis and accelerating wound closure. In conclusion, the hydrogel groups, especially the OSD/CMC/Fe/PA3 hydrogel + NIR and OSD/CMC/Fe/PA3 hydrogel groups, significantly reduced the production of pro-inflammatory factors (TNF- α) and promoted the production of VEGF, which in turn promoted wound healing, showing a higher repair effect than the control group.

3. Conclusion

In this study, a dual dynamic bond crosslinked hydrogel was constructed based on OSD and CMC with the catechol hydroxyl group in dopamine, carboxyl group in carboxymethyl chitosan and dynamic

metal coordination bonds of Fe³⁺. These hydrogels have good self-healing, adhesion and antioxidant properties. Besides, the addition of PA also endows the hydrogel with efficient antibacterial properties and suitable conductivity. In addition, good tissue adhesion makes these hydrogels more competitive in wound dressing applications. Radical scavenging experiments demonstrated the excellent antioxidant properties of the hydrogels. Obviously decreased blood loss in mouse liver injury proved that the hydrogel has good hemostatic properties. The experimental results of infected full-thickness skin wound repair in mice showed that the application of OSD/CMC/Fe/PA3 hydrogel with conductive and photothermal PA showed better wound closure with blood vessels, hair follicles and epidermis thickness closer to normal skin and less inflammation than commercial Tegaderm™ films and OSD/CMC hydrogel. In particular, immunofluorescence staining for TNF- α and VEGF during wound healing showed that these multifunctional hydrogels can reduce inflammation and increase vascular regeneration during wound repair. Taken together, all these results suggest that the multifunctional antibacterial conductive self-healing hydrogels with dual dynamic bonds are ideal candidates for infected wound dressings.

4. Materials and methods

4.1. Materials

Sodium alginate (SA) was obtained from Aladdin. Dopamine hydrochloride (DA) and 3-thienylacetic acid (TAA) was obtained from J&K. 1-(3-dimethylaminopropyl)-3-ethylcarbodiimide hydrochloride (EDC), N-hydroxysuccinyl imine (NHS) and carboxymethyl chitosan

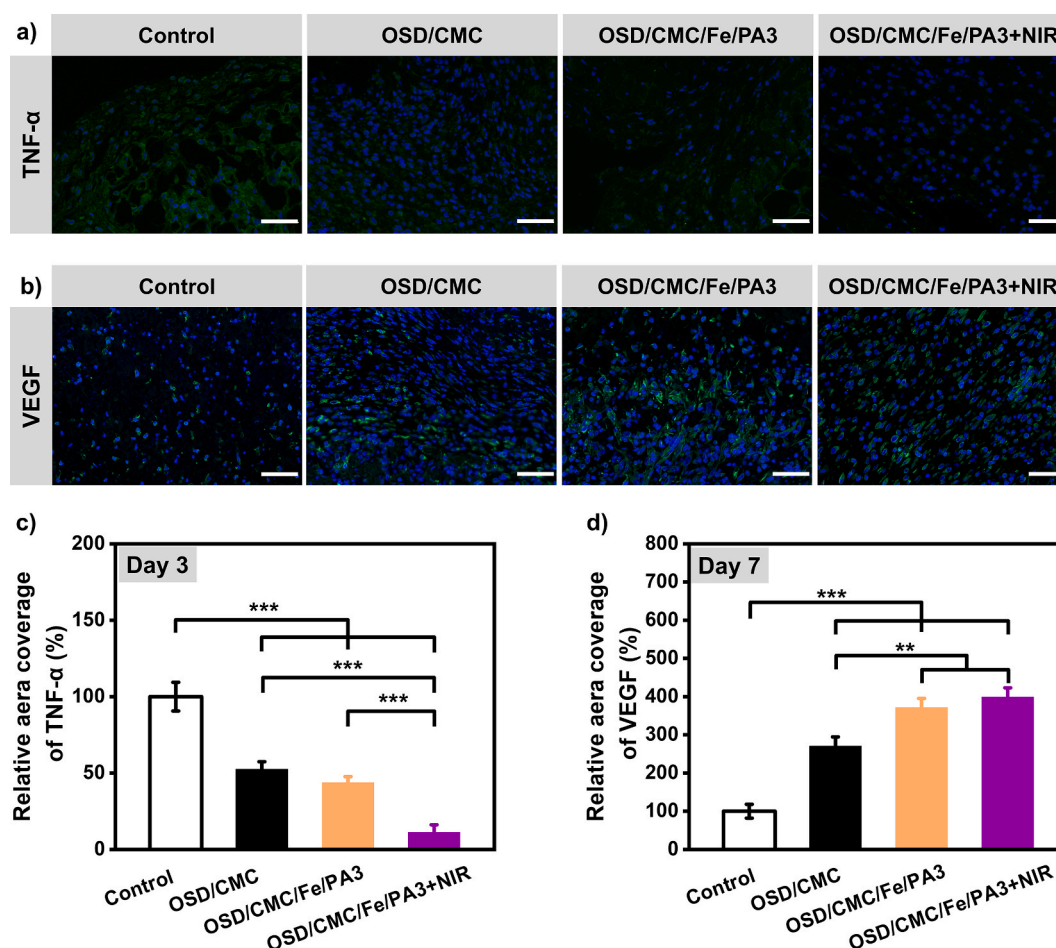


Fig. 8. Immunofluorescently labeled wound tissue with a) TNF- α (green) on day 3, Scale bar: 50 μ m; and b) VEGF (green) on day 7, Scale bar: 100 μ m; c) TNF- α and d) VEGF statistical data on the percentage of relative area covered, respectively. For all data, the control group was set at 100%. * $P < 0.05$, ** $P < 0.01$, *** $P < 0.001$.

(CMC) were obtained from Macklin. Sodium periodate (NaIO_4) and Ferric chloride were obtained from Sigma-Aldrich. The reagents were analytically pure and not further purified.

4.2. Synthesis of PA

PTAA was prepared according to literature using Fe^{3+} catalyzed coupling method. The specific processes are shown in Supporting Information (SI).

PA was prepared by stirring PTAA and DA hydrochloride together in an alkaline condition (Tris–HCl buffer, $\text{pH} = 8.5$). The specific processes are shown in SI.

4.3. Synthesis of OSD

OSA was prepared by the method of SA oxidation. OSD was prepared by grafting DA with EDC/NHS catalytic system. The specific processes are shown in SI.

4.4. Preparation of OSD/CMC/Fe/PA hydrogels

To prepare a 1 mL OSD/CMC/Fe/PA hydrogels, OSD was first dissolved in $\text{pH} = 7.4$ PBS to form a 15 wt% solution, CMC was dissolved in $\text{pH} = 7.4$ PBS to form a 9 wt% solution, Ferric chloride was dissolved in deionized water to form a 1 wt% solution, and PA was dispersed in PBS to form a 6 wt% dispersion. 400 μL of 15 wt% OSD solution was added, followed by 300 μL of 9 wt% CMC solution, 200 μL of 1 wt% Ferric chloride solution, and various amounts of deionized water and PA dispersion under constant stirring to form reddish-brown or black hydrogel. According to the presence or absence of Fe^{3+} and the amount of PA added, they were named as OSD/CMC, OSD/CMC/Fe, OSD/CMC/Fe/PA1 (1 wt% PA), OSD/CMC/Fe/PA3 (3 wt% PA), OSD/CMC/Fe/PA5 (5 wt% PA).

4.5. Characterizations of OSD/CMC/Fe/PA hydrogels

The nuclear magnetic resonance hydrogen spectroscopy (^1H NMR), Fourier transform infrared spectroscopy (FT-IR), UV–visible absorption spectroscopy (UV–vis), morphology observation, conductivity test, swelling test, in vitro degradation test, antioxidant properties, rheological tests and adhesion strength test were performed to study the physical and chemical properties of the hydrogel dressings [45,52]. The details are available in the SI.

4.6. Self-healing test of OSD/CMC/Fe/PA hydrogels

The self-healing performance test of hydrogel in rheology were tested with a TA rheometer (DHR-2) [53]. The exact procedure of the measurements is shown in the SI.

4.7. In vitro whole blood-clotting performance of OSD/CMC/Fe/PA hydrogels

The *In vitro* whole blood-clotting test was carried as the former method [35]. The exact procedure is described in SI.

4.8. Hemostasis performance of OSD/CMC/Fe/PA hydrogels

The hemostatic ability of OSD/CMC/Fe/PA hydrogels was tested using a mouse liver hemorrhage model (Kunming mice, 30–40 g, females) with reference to previous study [35]. The procedure is described in SI.

4.9. Hemolytic test of OSD/CMC/Fe/PA hydrogels

Hemocompatibility of the hydrogel was determined by hemolysis

test [35]. The exact procedure is described in SI.

4.10. Cytocompatibility test of OSD/CMC/Fe/PA hydrogels

The cytocompatibility test was carried out with the use of leachate method according to a previous study [35]. The exact procedure is described in SI.

4.11. Photothermal and photothermal antibacterial properties of OSD/CMC/Fe/PA hydrogels

The photothermal properties of OSD/CMC/Fe/PA hydrogels were evaluated by near-infrared (NIR) laser irradiation at 808 nm, and the photothermal antibacterial properties were measured according to the literature [14]. The whole exact procedure is described in SI.

4.12. In vivo MRSA-infected full-thickness skin wound healing evaluation of the OSD/CMC/Fe/PA hydrogels

Based on our previous study [14], a full-thickness skin defect model with MRSA infection was chosen to comprehensively assess the performance of the hydrogel dressing. The wound area was photographed on day 3, 7 and 14 and calculated by using Image J. The animal experiments were approved by the institutional review board of Xi'an Jiaotong University. The exact procedure is described in SI.

4.13. Histology and immunohistochemistry

Histological and immunohistochemical examinations were performed to evaluate vascular remodeling and inflammatory cells during wound healing. TNF- α and VEGF were chosen for immunohistochemical staining [14,51]. The exact procedure is described in SI.

4.14. Statistical analysis

For statistical analysis, the experimental data in this study were presented as mean \pm standard deviation and analyzed employing a Student's t-test. When the P value was less than 0.05, the data were considered to have significant difference [54].

Ethics approval

All protocols about animal experiments were approved by the animal research committee of Xi'an Jiaotong University.

CRediT authorship contribution statement

Lipeng Qiao: Investigation, Methodology, Data curation, Writing – original draft. **Yongping Liang:** Conducted most of the animal experiments, Formal analysis. **Jueying Chen:** Conducted the antibacterial test, Formal analysis. **Ying Huang:** Writing – review & editing. **Saeed A. Alsareii:** Project administration, Funding acquisition. **Abdulrahman Manaa Alamri:** Validation, Supervision, Funding acquisition. **Farid A. Harraz:** Methodology, Investigation. **Baolin Guo:** Conceptualization, Methodology, Writing – review & editing, Supervision, Funding acquisition.

Declaration of competing interest

The authors declare that they have no competing interests.

Acknowledgments

The authors are thankful to the Deanship of Scientific Research at Najran University for funding this work, under the Research Groups Funding Program grant code (NU/RG/MRC/12/5). This work was

jointly supported by the National Natural Science Foundation of China (grant numbers: 51973172, 52273149), Supported by 111 Project 2.0 (BPO618008), the Natural Science Foundation of Shaanxi Province (No. 2020JC-03), State Key Laboratory for Mechanical Behavior of Materials, and the World-Class Universities (Disciplines) and the Characteristic Development Guidance Funds for the Central Universities. We also thank Instrument Analysis Center of Xi'an Jiaotong University for their assistance with XPS analysis.

Appendix A. Supplementary data

Supplementary data to this article can be found online at <https://doi.org/10.1016/j.bioactmat.2023.07.015>.

References

- O. Castaño, S. Pérez-Amodio, C. Navarro-Requena, M.Á. Mateos-Timoneda, E. Engel, Instructive microenvironments in skin wound healing: biomaterials as signal releasing platforms, *Adv. Drug Deliv. Rev.* 129 (2018) 95–117.
- M. Wang, Y. Luo, T. Wang, C. Wan, L. Pan, S. Pan, K. He, A. Neo, X. Chen, Artificial skin perception, *Adv. Mater.* 33 (19) (2021), 2003014.
- X. Zhao, Y. Liang, Y. Huang, J. He, Y. Han, B. Guo, Physical double-network hydrogel adhesives with rapid shape adaptability, fast self-healing, antioxidant and NIR/pH stimulus-responsiveness for multidrug-resistant bacterial infection and removable wound dressing, *Adv. Funct. Mater.* 30 (17) (2020), 1910748.
- A.D. Schoenenberger, H. Tempfer, C. Lehner, J. Egloff, M. Mauracher, A. Bird, R. Widmer, K. Maniura-Weber, S.F. Fucentese, A. Traweger, U. Silvan, J. G. Sneider, Macromechanics and polycaprolactone fiber organization drive macrophage polarization and regulate inflammatory activation of tendon in vitro and in vivo, *Biomaterials* 249 (2020), 120034.
- X. Wei, S. Ding, S. Liu, K. Yang, J. Cai, F. Li, C. Wang, S. Lin, F. Tian, Polysaccharides-modified chitosan as improved and rapid hemostasis foam sponges, *Carbohydr. Polym.* 264 (2021), 118028.
- M.F.P. Graça, S.P. Miguel, C.S.D. Cabral, L.J. Correia, Hyaluronic acid–based wound dressings: a review, *Carbohydr. Polym.* 241 (2020), 116364.
- M. Alizadehgiashi, C.R. Nemr, M. Chekini, D. Pinto Ramos, N. Mittal, S.U. Ahmed, N. Khuu, S.O. Kelley, E. Kumacheva, Multifunctional 3D-printed wound dressings, *ACS Nano* 15 (7) (2021) 12375–12387.
- S. Talebian, M. Mehrli, N. Taebnia, C.P. Pennisi, F.B. Kadumudi, J. Foroughi, M. Hasany, M. Nikkhah, M. Akbari, G. Orive, A. Dolatshahi-Pirouz, Self-healing hydrogels: the next paradigm shift in tissue engineering? *Adv. Sci.* 6 (16) (2019), 1801664.
- Y. Yang, M.W. Urban, Self-healing polymeric materials, *Chem. Soc. Rev.* 42 (17) (2013) 7446–7467.
- Y. Li, J. Wen, M. Qin, Y. Cao, H. Ma, W. Wang, Single-molecule mechanics of catechol-iron coordination bonds, *ACS Biomater. Sci. Eng.* 3 (6) (2017) 979–989.
- X. Dou, Q. Zhou, X. Chen, Y. Tan, X. He, P. Lu, K. Sui, B.Z. Tang, Y. Zhang, W. Z. Yuan, Clustering-triggered emission and persistent room temperature phosphorescence of sodium alginate, *Biomacromolecules* 19 (6) (2018) 2014–2022.
- W. Yang, X. Wu, F. Liu, Y. Dou, Z. Hu, W. Hao, A fluorescent, self-healing and pH sensitive hydrogel rapidly fabricated from HPAMAM and oxidized alginate with injectability, *RSC Adv.* 6 (41) (2016) 34254–34260.
- H. Zhou, C.C. Mayorga-Martinez, M. Pumera, Microplastic removal and degradation by mussel-inspired adhesive magnetic/enzymatic microrobots, *Small Methods* 5 (9) (2021), 2100230.
- Y. Liang, X. Zhao, T. Hu, B. Chen, Z. Yin, P.X. Ma, B. Guo, Adhesive hemostatic conducting injectable composite hydrogels with sustained drug release and photothermal antibacterial activity to promote full-thickness skin regeneration during wound healing, *Small* 15 (12) (2019), 1900046.
- M. Linhorst, J. Wattjes, B.M. Moerschbacher, Chitin deacetylase as a biocatalyst for the selective N-acylation of chitosan oligo- and polymers, *ACS Catal.* 11 (23) (2021) 14456–14466.
- W. Wang, C. Xue, X. Mao, Chitosan: structural modification, biological activity and application, *Int. J. Biol. Macromol.* 164 (2020) 4532–4546.
- P. Chan, M. Kurisawa, J.E. Chung, Y.-Y. Yang, Synthesis and characterization of chitosan-g-poly(ethylene glycol)-folate as a non-viral carrier for tumor-targeted gene delivery, *Biomaterials* 28 (3) (2007) 540–549.
- X. Zhang, Z. Si, Y. Wang, Y. Li, C. Xu, H. Tian, Polymerization and coordination synergistically constructed photothermal agents for macrophages-mediated tumor targeting diagnosis and therapy, *Biomaterials* 264 (2021), 120382.
- J. Wang, J. Lu, Y. Zhou, Y. Zhou, Multifunctional antibacterial materials for the control of hazardous microbes and chemicals: a review, *ACS ES&T Mater* 1 (3) (2021) 479–497.
- P. Makvandi, C.-y. Wang, E.N. Zare, A. Borzacchiello, L.-n. Niu, F.R. Tay, Metal-based nanomaterials in biomedical applications: antimicrobial activity and cytotoxicity aspects, *Adv. Funct. Mater.* 30 (22) (2020), 1910021.
- D. Banerjee, P.M. Shivapriya, P.K. Gautam, K. Misra, A.K. Sahoo, S.K. Samanta, A review on basic biology of bacterial biofilm infections and their treatments by nanotechnology-based approaches, *Proc. Natl. Acad. Sci. India Sect. B (Biol. Sci.)* 90 (2) (2020) 243–259.
- Y.-Q. Zhao, Y. Sun, Y. Zhang, X. Ding, N. Zhao, B. Yu, H. Zhao, S. Duan, F.-J. Xu, Well-defined gold nanorod/polymer hybrid coating with inherent antifouling and photothermal bactericidal properties for treating an infected hernia, *ACS Nano* 14 (2) (2020) 2265–2275.
- D. Li, Y.-p. Wen, J.-k. Xu, H.-h. He, M. Liu, An amperometric biosensor based on covalent immobilization of ascorbate oxidase on biocompatible and low-toxic poly(thiophene-3-acetic acid) matrix, *Chin. J. Polym. Sci.* 30 (5) (2012) 705–718.
- B. Yang, F. Yao, T. Hao, W. Fang, L. Ye, Y. Zhang, Y. Wang, J. Li, C. Wang, Development of electrically conductive double-network hydrogels via one-step facile strategy for cardiac tissue engineering, *Adv. Healthcare Mater.* 5 (4) (2016) 474–488.
- R. Yu, H. Zhang, B. Guo, Conductive biomaterials as bioactive wound dressing for wound healing and skin tissue engineering, *Nano-Micro Lett.* 14 (1) (2021) 1.
- T. Jayaramudu, H.-U. Ko, H.C. Kim, J.W. Kim, J. Kim, Swelling behavior of polyacrylamide–cellulose nanocrystal hydrogels: swelling kinetics, temperature, and pH effects, *Materials* 12 (13) (2019).
- S. Liu, Q. Zhang, J. Yu, N. Shao, H. Lu, J. Guo, X. Qiu, D. Zhou, Y. Huang, Absorbable thioether grafted hyaluronic acid nanofibrous hydrogel for synergistic modulation of inflammation microenvironment to accelerate chronic diabetic wound healing, *Adv. Healthcare Mater.* 9 (11) (2020), 2000198.
- K.S. Munir, C. Wen, Y. Li, Carbon nanotubes and graphene as nanoreinforcements in metallic biomaterials: a review, *Adv. Biosyst.* 3 (3) (2019), 1800212.
- M. Chen, J. Tian, Y. Liu, H. Cao, R. Li, J. Wang, J. Wu, Q. Zhang, Dynamic covalent constructed self-healing hydrogel for sequential delivery of antibacterial agent and growth factor in wound healing, *Chem. Eng. J.* 373 (2019) 413–424.
- J. Ren, H. Xuan, W. Dai, Y. Zhu, L. Ge, Double network self-healing film based on metal chelation and Schiff-base interaction and its biological activities, *Appl. Surf. Sci.* 448 (2018) 609–617.
- H. Huang, Z. Dong, X. Ren, B. Jia, G. Li, S. Zhou, X. Zhao, W. Wang, High-strength hydrogels: fabrication, reinforcement mechanisms, and applications, *Nano Res.* 16 (2) (2023) 3475–3515.
- Y. Huang, X. Zhao, C. Wang, J. Chen, Y. Liang, Z. Li, Y. Han, B. Guo, High-strength anti-bacterial composite cryogel for lethal noncompressible hemorrhage hemostasis: synergistic physical hemostasis and chemical hemostasis, *Chem. Eng. J.* 427 (2022), 131977.
- Z. Xu, S. Han, Z. Gu, J. Wu, Advances and impact of antioxidant hydrogel in chronic wound healing, *Adv. Healthcare Mater.* 9 (5) (2020), 1901502.
- D. Gopinath, M.R. Ahmed, K. Gomathi, K. Chitra, P.K. Sehgal, R. Jayakumar, Dermal wound healing processes with curcumin incorporated collagen films, *Biomaterials* 25 (10) (2004) 1911–1917.
- M. Li, Y. Liang, Y. Liang, G. Pan, B. Guo, Injectable stretchable self-healing dual dynamic network hydrogel as adhesive anti-oxidant wound dressing for photothermal clearance of bacteria and promoting wound healing of MRSA infected motion wounds, *Chem. Eng. J.* 427 (2022), 132039.
- N. Sahiner, S. Sagbas, M. Sahiner, D.A. Blake, W.F. Reed, Polydopamine particles as nontoxic, blood compatible, antioxidant and drug delivery materials, *Colloids Surf., B* 172 (2018) 618–626.
- W. Zhang, R. Wang, Z. Sun, X. Zhu, Q. Zhao, T. Zhang, A. Cholewinski, F. Yang, B. Zhao, R. Pinnaratip, P.K. Forooshani, B.P. Lee, Catechol-functionalized hydrogels: biomimetic design, adhesion mechanism, and biomedical applications, *Chem. Soc. Rev.* 49 (2) (2020) 433–464.
- H. Guo, S. Huang, A. Xu, W. Xue, Injectable adhesive self-healing multiple-dynamic-bond crosslinked hydrogel with photothermal antibacterial activity for infected wound healing, *Chem. Mater.* 34 (6) (2022) 2655–2671.
- C. Cui, W. Liu, Recent advances in wet adhesives: adhesion mechanism, design principle and applications, *Prog. Polym. Sci.* 116 (2021), 101388.
- X. Fan, Y. Fang, W. Zhou, L. Yan, Y. Xu, H. Zhu, H. Liu, Mussel foot protein inspired tough tissue-selective underwater adhesive hydrogel, *Mater. Horiz.* 8 (3) (2021) 997–1007.
- C. Zhang, M. Wang, C. Jiang, P. Zhu, B. Sun, Q. Gao, C. Gao, R. Liu, Highly adhesive and self-healing γ -PGA/PEDOT:PSS conductive hydrogels enabled by multiple hydrogen bonding for wearable electronics, *Nano Energy* 95 (2022), 106991.
- Y. Liang, J. He, B. Guo, Functional hydrogels as wound dressing to enhance wound healing, *ACS Nano* 15 (8) (2021) 12687–12722.
- X. Zhao, H. Wu, B. Guo, R. Dong, Y. Qiu, P.X. Ma, Antibacterial anti-oxidant electroactive injectable hydrogel as self-healing wound dressing with hemostasis and adhesiveness for cutaneous wound healing, *Biomaterials* 122 (2017) 34–47.
- J. Chen, Y. Liu, G. Cheng, J. Guo, S. Du, J. Qiu, C. Wang, C. Li, X. Yang, T. Chen, Z. Chen, Tailored hydrogel delivering niobium carbide boosts ROS-scavenging and antimicrobial activities for diabetic wound healing, *Small* 18 (27) (2022), 2201300.
- X. Zhao, Z. Zhang, J. Luo, Z. Wu, Z. Yang, S. Zhou, Y. Tu, Y. Huang, Y. Han, B. Guo, Biomimetic, highly elastic conductive and hemostatic gelatin/rGO-based nanocomposite cryogel to improve 3D myogenic differentiation and guide in vivo skeletal muscle regeneration, *Appl. Mater. Today* 26 (2022), 101365.
- Z. Guo, Z. Zhang, N. Zhang, W. Gao, J. Li, Y. Pu, B. He, J. Xie, A Mg²⁺/polydopamine composite hydrogel for the acceleration of infected wound healing, *Bioact. Mater.* 15 (2022) 203–213.
- P. Zhao, Y. Zhang, X. Chen, C. Xu, J. Guo, M. Deng, X. Qu, P. Huang, Z. Feng, J. Zhang, Versatile hydrogel dressing with skin adaptiveness and mild photothermal antibacterial activity for methicillin-resistant *Staphylococcus aureus*-infected dynamic wound healing, *Adv. Sci.* 10 (11) (2023), 2206585.
- X. Yin, Y. Hao, Y. Lu, D. Zhang, Y. Zhao, L. Mei, K. Sui, Q. Zhou, J. Hu, Multifunctional hydrogel patches for repairing full-thickness abdominal wall defects, *Adv. Funct. Mater.* 31 (41) (2021), 2105614.

- [49] L. Wang, X. Zhang, K. Yang, Y.V. Fu, T. Xu, S. Li, D. Zhang, L.-N. Wang, C.-S. Lee, A novel double-crosslinking-double-network design for injectable hydrogels with enhanced tissue adhesion and antibacterial capability for wound treatment, *Adv. Funct. Mater.* 30 (1) (2020), 1904156.
- [50] B. Saleh, H.K. Dhaliwal, R. Portillo-Lara, E. Shirzaei Sani, R. Abdi, M.M. Amiji, N. Annabi, Local immunomodulation using an adhesive hydrogel loaded with miRNA-laden nanoparticles promotes wound healing, *Small* 15 (36) (2019), 1902232.
- [51] N. Ferrara, VEGF and the quest for tumour angiogenesis factors, *Nat. Rev. Cancer* 2 (10) (2002) 795–803.
- [52] Y. Liang, Z. Li, Y. Huang, R. Yu, B. Guo, Dual-dynamic-bond cross-linked antibacterial adhesive hydrogel sealants with on-demand removability for post-wound-closure and infected wound healing, *ACS Nano* 15 (4) (2021) 7078–7093.
- [53] J. Qu, X. Zhao, Y. Liang, T. Zhang, P.X. Ma, B. Guo, Antibacterial adhesive injectable hydrogels with rapid self-healing, extensibility and compressibility as wound dressing for joints skin wound healing, *Biomaterials* 183 (2018) 185–199.
- [54] S. Kam Nadine Wong, M. O'Connell, A. Wisdom Jeffrey, H. Dai, Carbon nanotubes as multifunctional biological transporters and near-infrared agents for selective cancer cell destruction, *Proc. Natl. Acad. Sci. USA* 102 (33) (2005) 11600–11605.